Structural and Magnetic Properties of $M(mnt)_2$ Salts (M = Ni, Pt, Cu) with a Ferrocene-Based Cation, $[FcCH_2N(CH_3)_3]^+$. Interplay between M···M and M···S Intermolecular Interactions

Anthony E. Pullen,[†] Christophe Faulmann,[†] Konstantin I. Pokhodnya,*[,†] Patrick Cassoux,*[,†] and Madoka Tokumoto[‡]

Equipe Précurseurs Moléculaires et Matériaux, LCC-CNRS, 205 Route de Narbonne, 31077 Toulouse Cédex, France, and Electrotechnical Laboratory, 1-1-4 Umezono, Tsukuba, Ibaraki 305, Japan

Received July 24, 1998

A series of metal bis-mnt complexes (mnt = 1,2-dithiolatomaleonitrile) with the trimethylammonium methylferrocene cation have been synthesized and characterized using X-ray diffraction, magnetic susceptibility, and differential scanning calorimetry measurements. The complexes have the formulas $(FcCH_2NMe_3)[Ni(mnt)_2]$ (**2**), $(FcCH_2NMe_3)[Pt(mnt)_2]$ (**3**), and $(FcCH_2NMe_3)_2[Cu(mnt)_2]$ (**4**) (where Fc = ferrocene). At 300 K, the crystal structures of 1:1 complexes **2** and **3** are very similar. They consist of pairs of $[M(mnt)_2]^-$ in a slipped configuration packed in stacks. Each $[M(mnt)_2]^-$ stack is separated from adjacent stacks by two columns of cations. Within the pairs, the $[M(mnt)_2]^-$ anions interact via short M···S contacts, while there are no short contacts between the pairs. Complex **4**, which has a 2:1 stoichiometry, exhibits a markedly different packing arrangement of the anionic units. Due to the special position of the Cu atom in the asymmetric unit cell, $[Cu(mnt)_2]^{2-}$ dianions are completely isolated from each other. The magnetic susceptibility behavior of the nickel complex is consistent with the presence of magnetically isolated, antiferromagnetically (AF) coupled $[Ni(mnt)_2]^-$ pairs with the AF exchange parameter, $J = -840$ cm^{-1}. The platinum complex undergoes an endothermic structural phase transition (T_p) at 247 K. Below T_p its structure is characterized by the formation of magnetically isolated $[Pt(mnt)_2]_2^{2-}$ dimers in an eclipsed configuration with short Pt···Pt and S···S contacts between monomers. In the magnetic properties, the structural changes reveal themselves as an abrupt susceptibility drop implying a substantial increase of the AF exchange parameter. A mechanism of the phase transition in the platinum compound is proposed. For compound **4**, paramagnetic behavior is observed.

Introduction

Among the strategies developed for the synthesis of molecular magnets,[1] special attention has been given to charge-transfer (CT) complexes. Metal dithiolenes $M(mnt)_2$ (M = Ni, Pt, Pd; mnt = $S_2C_4N_2^{2-}$ = dithiolatomaleonitrile), which are planar electronic acceptors (A), were widely used for the synthesis of CT compounds with unusual magnetic properties.[2−6] It is well-known that $M(mnt)_2$ salts of bulky cations (e.g., NEt_4) crystallize in columnar like structures containing $[M(mnt)_2]^-$ pairs (or "dimers") in a slipped configuration such that the central metal atom is positioned above the S atom of the other anion.[7,8] On the other hand, it has been shown that $M(mnt)_2$ complexes with organometallic ferrocene-based cation radicals (D) possess either an alternating ···$D^+A^-A^-D^+D^+A^-A^-D^+$··· stack or segregated, D^+ and A^-, stack packing arrangement in which $M(mnt)_2$ dimers are in an eclipsed configuration.[2,4] For both arrangements, an $S = 0$ ground state was reported for the $[M(mnt)_2]_2^{2-}$ dimers. The magnetic behavior of these compounds on cooling was ascribed to a progressive thermal depopulation of the excited triplet state of the $[M(mnt)_2]_2^{2-}$ dimers and a paramagnetic contribution from isolated ferrocene-based cation radicals.[2]

The recent discovery of a ferromagnetic ordering in $(NH_4)[Ni(mnt)_2)]\cdot H_2O$ (**1**) below 4.5 K[5] has stimulated renewed interest in $M(mnt)_2$-based compounds, since the unusual magnetic behavior in **1** is totally attributed to the anionic part. The crystal structure of this salt consists of eclipsed equidistant stacks of anions, with an indication of dimerization within the stacks below 98 K. One can assume that the dimerized structure of the $M(mnt)_2$ stacks does not necessarily suppress the ferromagnetic-like ordering. On the other hand, the distinctive feature of this salt is a considerable interaction between $Ni(mnt)_2$ columns via a network of hydrogen bonds which might be one of the reasons of the unusual magnetic behavior.[6]

* To whom correspondence should be addressed. E-mail address: cassoux@lcc-toulouse.fr.
[†] LCC-CNRS.
[‡] Electrotechnical Laboratory.

(1) (a) Stumpf, H. O.; Ouahab, L.; Pei, Y.; Bergerat, P.; Kahn, O. *J. Am. Chem. Soc.* **1994**, *116*, 3866−3874. (b) Miller, J. S.; Epstein, A. J. *Angew. Chem., Int. Ed. Engl.* **1994**, *33*, 385−415.
(2) Miller, J. S.; Calabrese, J. C.; Epstein, A. J. *Inorg. Chem.* **1989**, *28*, 0−4238.
(3) Fettouhi, M.; Ouahab, L.; Hagiwara, M.; Codjovi, E.; Kahn, O.; Constant-Machado, H.; Varret, F. *Inorg. Chem.* **1995**, *34*, 4152−4159.
(4) Hobi, M.; Zürcher, S.; Granlich, V.; Burckhardt, U.; Mensing, C.; Spahr, M.; Togni, A. *Organometallics* **1996**, *15*, 5342−5346.
(5) Coomber, A. T.; Beljonne, D.; Friend, R. H.; Brédas, J. L.; Charlton, A.; Robertson, N.; Underhill, A. E.; Kurmoo, M.; Day, P. *Nature* **1996**, *380*, 144−146.
(6) Allan, M. L.; Coomber, A. T.; Marsden, I. R.; Martens, J. H. F.; Friend, R. H.; Charlton, A.; Underhill, A. E. *Synth. Met.* **1993**, *55*−*57*, 3317−3322.
(7) Clemenson, P. I.; Underhill, A. E.; Hursthouse, M. B.; Short, R. L. *J. Chem. Soc., Dalton Trans.* **1988**, 1689−1691.
(8) Kobayashi, A.; Sasaki, Y. *Bull. Chem. Soc. Jpn.* **1977**, *50*, 2650−2656.

10.1021/ic980876v CCC: $15.00
Published on Web 12/03/1998

Table 1. Crystallographic Data for Complexes **2**−**4**

	2	**3**		**4**
molecular formula	$C_{22}H_{20}FeNiS_4N_5$	$C_{22}H_{20}FePtS_4N_5$	$C_{22}H_{20}FePtS_4N_5$	$C_{36}H_{40}Fe_2CuS_4N_6$
M	597.3	733.6	733.6	860.3
space group (no.)	$P2_1/n$ (14)	$P2_1/n$ (14)	$P2_1/n$ (14)	$P2_1/n$ (14)
a/Å	12.116(2)	12.119(4)	12.183(1)	12.804(1)
b/Å	30.094(16)	30.112(4)	29.667(3)	10.036(1)
c/Å	7.139(6)	7.244(4)	7.268(1)	15.971(2)
β/deg	103.50(3)	103.97(4)	105.54(1)	109.81(1)
V/Å^3	2531(3)	2565(2)	2531(1)	1931(1)
Z	4	4	4	2
μ/cm^{-1}	16.6	64.5	64.5	15.4
T/°C	20	20	−113	−113
λ, Å	0.710 73	0.710 73	0.710 73	0.710 73
ρ_c/g cm^{-3}	1.57	1.93	1.93	1.48
R^a	0.046	0.051	0.024	0.036
R' [a]	0.033	0.042	0.020	0.033

[a] $R(F_o) = \sum(||F_o| - |F_c||)/\sum|F_o|$ and $R'(F_o) = [\sum w(|F_o| - |F_c|)^2/\sum wF_o^2]^{1/2}$.

Table 2. Intermolecular Interatomic Distances (Å) Involving M and S Atoms in Compounds **2** and **3**

	2		**3** (295 K)		**3** (160 K)	
overlap	(AB)	(BA′)	(AB)	(BA′)	(AB)	(BA′)
M−M	4.275	3.872	4.339	3.824	4.418	3.451
M−S(4)	3.648	3.527	3.688	3.626	3.618	3.913
S(i)−S(j)	S(3)−S(4)	S(1)−S(4)	S(3)−S(4)	S(1)−S(4)	S(3)−S(4)	S(1)−S(4) 3.408
	3.565	3.795	3.640	3.770	3.766	S(2)−S(3) 3.534

[a] Symmetry operation applied on second atom for (AB) overlap, $1-x, -y, 1-z$; for (BA′) overlap, $1-x, -y, 2-z$.

To induce or enhance intermolecular interactions as seen in compound **1** which results in its cooperative magnetic behavior, we have chosen to combine a paramagnetic $[M(mnt)_2]^-$ anion with a diamagnetic closed-shell cation. The cation consists of a ferrocene with a covalently attached methyl trimethylammonium pendant group, $[FcCH_2NMe_3]^+$. In this work, we present the synthesis, structural characterization, and magnetic properties of the 1:1 complexes $(FcCH_2NMe_3)[Ni(mnt)_2]$ (**2**) and $(FcCH_2NMe_3)[Pt(mnt)_2]$ (**3**) and the 2:1 complex $(FcCH_2NMe_3)_2[Cu(mnt)_2]$ (**4**).

Experimental Section

General Procedures. All manipulations were carried out in air unless otherwise noted. All organic solvents were purified according to standard procedures. The compounds $(Bu_4N)[Ni(mnt)_2]$, $(Bu_4N)[Pt(mnt)_2]$, and Na_2mnt were synthesized following the procedures found in ref 9, and $FcCH_2NMe_3CF_3SO_3$ was synthesized following Veya et al.[10] Elemental analyses were completed at the LCC−CNRS, Toulouse.

Preparation of $(FcCH_2NMe_3)[Ni(mnt)_2]$ (2). A solution of 58 mg (0.10 mmol) of $(Bu_4N)[Ni(mnt)_2]$ in a minimal amount of CH_3CN was added quickly without agitation to a solution of 41 mg (0.10 mmol) of $FcCH_2NMe_3CF_3SO_3$ in a minimal amount of CH_3CN. The mixture was allowed to stand in air. Evaporation of the solvent over a period of 5−6 h yielded black chunk-like crystals. They were filtered, and washed with methanol followed by ether, and air-dried to yield 55 mg (92%) of $(FcCH_2NMe_3)[Ni(mnt)_2]$ (**2**) as black needles. Anal. Found (calcd for $C_{22}H_{20}FeNiN_5S_4$): C, 44.10 (44.25); H, 3.31 (3.38); N, 11.70 (11.73).

$(FcCH_2NMe_3)[Pt(mnt)_2]$ (3). Complex **3** was synthesized similar to **2**. A solution of 72 mg (0.10 mmol) of $(Bu_4N)[Pt(mnt)_2]$ and a solution of 41 mg (0.10 mmol) of $FcCH_2NMe_3CF_3SO_3$ in minimal amounts of CH_3CN were combined without stirring. Black chunk-like crystals formed upon evaporation of the solvent. They were filtered, washed with methanol and ether, and air-dried to yield 56 mg (77%) of $(FcCH_2NMe_3)[Pt(mnt)_2]$ (**3**) as black needles. Anal. Found (calcd for $C_{22}H_{20}FePtN_5S_4$): C, 36.13 (36.02); H, 2.28 (2.75); N, 9.81 (9.55).

$(FcCH_2NMe_3)_2[Cu(mnt)_2]$ (4). In a two-neck flask equipped with a stir bar and argon inlet was placed 0.50 g (2.68×10^{-3} mol) of Na_2mnt, which was dissolved in 10 mL of a 1:1 mixture of EtOH/water. To this was added a solution of 0.22 g (1.34×10^{-3} mol) of $CuSO_4$ in 10 mL of water and stirred for 10 min. A 15 mL aqueous solution of 1.20 g (2.96×10^{-3} mol) of $FcCH_2NMe_3CF_3SO_3$ was added, and a deep red-brown precipitate formed. The precipitate was filtered, washed with methanol and ether, and crystallized from acetone/2-propanol. Crystals for X-ray were obtained from an evaporated solution of acetone/2-propanol in air. Large red-brown platelets of $(FcCH_2NMe_3)_2[Cu(mnt)_2]$ (**4**) formed (0.95 g, 82%). Anal. Found (calcd for $C_{36}H_{40}CuFe_2N_6S_4$): C, 50.30 (50.26); H, 3.97 (4.69); N, 9.50 (9.77).

X-ray Crystallography. Crystallographic data for compounds $(FcCH_2NMe_3)[Ni(mnt)_2]$ (**2**), $(FcCH_2NMe_3)[Pt(mnt)_2]$ (**3**) (at room temperature and 160 K), and $(FcCH_2NMe_3)_2[Cu(mnt)_2]$ (**4**) are presented in Table 1 along with selected data collection and processing parameters. Selected M···M, M···S, and S···S intermolecular distances for compounds **2** and **3** are located in Table 2.

At room-temperature, an Enraf-Nonius CAD4 diffractometer was used for the data collection ($\omega/2\theta$ mode) of $(FcCH_2NMe_3)[Ni(mnt)_2]$ (**2**) and $(FcCH_2NMe_3)[Pt(mnt)_2]$ (**3**). The cell parameters were determined by least-squares refinement on diffractometer angles from 18 reflections, $6° < \theta < 10°$ for **2** and from 25 reflections, $6° < \theta < 11°$ for **3**. The intensity of three reflections was monitored throughout the data collection, and no significant decay was observed. An empirical absorption correction based on ψ scan[11] was applied (minimum and maximum transmission factors: 0.630, 0.864 for **2**, and 0.518, 0.741 for **3**). At 160 K, an imaging plate IPDS−STOE diffractometer was used for the data collection (ϕ-scan) of $(FcCH_2NMe_3)[Pt(mnt)_2]$ (**3**) and $(FcCH_2NMe_3)_2[Cu(mnt)_2]$ (**4**). The cell parameters were determined from 5000 reflections, with $2° < \theta < 24°$. Numerical absorption corrections[12] were applied to the data set (minimum and maximum transmission factors: 0.313, 0.502 for **3** and 0.534, 0.939 for **4**). Data for all structures were corrected for Lorentz−polarization effects.

For every compound, the structures were solved by direct methods (SHELXS-86)[13] followed by normal heavy-atom procedures. For

(9) Davison, A., Holm, R. H. *Inorg. Synth.* **1967**, *10*, 8−26.
(10) Veya, L.; Kochi, J. K. *J. Organomet. Chem.* **1995**, *488*, C4−C8.
(11) North, A. C. T.; Phillips, D. C.; Mathews, F. S. *Acta Crystallogr., Sect. A* **1968**, *24*, 351−359.
(12) *X-Shape, version 1.01, Crystal Optimisation for Numerical Absorption Correction*; STOE and Cie GmbH: Darmstadt, 1996.

($FcCH_2NMe_3$)[Ni(mnt)$_2$] (**2**), full-matrix least-squares refinement with all non-H atoms anisotropic except the C atoms of the disordered C_5H_5 ring and hydrogen atoms calculated, not refined but included in the calculations. A five-parameter Chebychev weighting scheme[14] was applied to the structure. For ($FcCH_2NMe_3$)[Pt(mnt)$_2$] (**3**), full-matrix least-squares refinement with all atoms anisotropic except the C atoms of the cation. Hydrogen atoms calculated, not refined but included in the calculations. A four-parameter Chebychev weighting scheme[14] was applied to the structure. At 160 K, for ($FcCH_2NMe_3$)[Pt(mnt)$_2$] (**3**) and ($FcCH_2NMe_3$)$_2$[Cu(mnt)$_2$] (**4**), full-matrix least-squares refinement was performed with all non-H atoms anisotropic. Hydrogen atoms calculated and not refined for **3** and only coordinates refined for **4**. Three- and five-parameter Chebychev weighting schemes[14] were applied to the structures of **3** and **4**, respectively. All crystallographic calculations were performed using the Crystals package.[15] Neutral atom scattering factors were taken from ref 16.

Magnetic Susceptibility. Magnetic susceptibilities for polycrystalline pressed pellet samples were measured at the external field of 0.1 T using a MPMS (Quantum Design) SQUID magnetometer. The background was obtained over the full temperature range prior to measuring the samples. Sample amount varied from 20 to 30 mg. To exclude the oxygen contamination, the sample compartment was evacuated and then filled with helium gas.

ESR Spectroscopy. The ESR spectra of ($FcCH_2NMe_3$)[Ni(mnt)$_2$] (**2**) single crystals were recorded with a Brüker ESP 300E instrument equipped with a Brüker ER 035M gaussmeter and an EIP 548 microwave frequency counter operating at X-band in the temperature range of 100−300 K.

Differential Scanning Calorimetry (DSC). DSC experiments were performed with a SETARAM DSC 131 calorimeter. Thermal analysis of a polycrystalline sample placed in an aluminum crucible was carried out on warming (rate 10 K/min) in the temperature range of −80 to 120 °C (193−393 K).

Results and Discussion

Crystal Structures. The anionic [M(mnt)$_2$]$^{n-}$ entities (n = 1 or 2) for all compounds are nearly planar; the largest out-of-plane deviations were observed for the terminal N atoms of **2** and **3** (0.138, 0.139 (300 K) and 0.174 Å (160 K)) and for the S(2) atom of compound **4** (0.147 Å). The asymmetric unit and the labeling used for compounds ($FcCH_2NMe_3$)[Ni(mnt)$_2$] (**2**), ($FcCH_2NMe_3$)[Pt(mnt)$_2$] (**3**), and ($FcCH_2NMe_3$)$_2$[Cu(mnt)$_2$] (**4**) are shown in Figures 1 and 2.

At room-temperature compounds **2** and **3** are isostructural. They both form columns of [M(mnt)$_2$]$^-$ anions along the c direction which are separated by 2 columns of cations (Figure 3a and b). The cations are arranged in such a way that the dimethylamino groups are pointed in opposite directions (Figure 3b). No close intermolecular contacts were found between the adjacent cationic and anionic columns.

For complexes **2** and **3**, the [M(mnt)$_2$]$^-$ planes are parallel within the columns and are canted in an alternating fashion from column to column along directions [1 1 0] and [1 $\bar{1}$ 0]. The perpendicular to the plane of the [M(mnt)$_2$]$^-$ entities within the columns form an angle of ±12.9° or ±13.8° with the c direction in **2** and **3**, respectively. The central metal atoms are positioned inversely symmetrically with respect to the *ac* and *ab* planes in an alternating zigzag fashion (A−B−A′). The distance between the central metal atoms of the anions A and B is equal to 4.275 or 4.339 Å, while this distance between anions B and A′ is 3.872 and 3.824 Å for the complexes **2** and **3**, respectively (Table 2). Both of these values are beyond the metal−metal bonding distances.

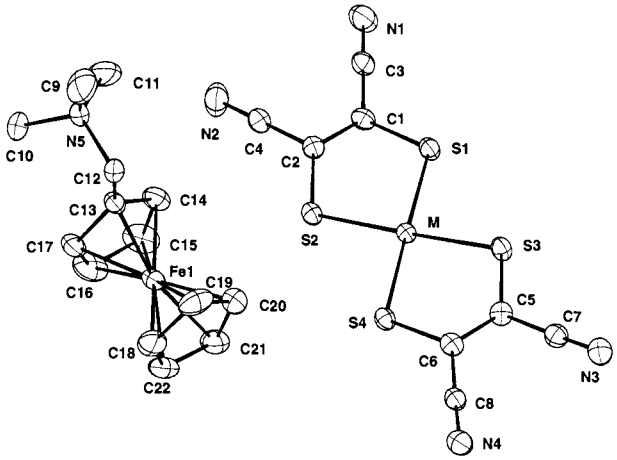

Figure 1. Atomic numbering scheme for ($FcCH_2NMe_3$)[Ni(mnt)$_2$] (**2**) and ($FcCH_2NMe_3$)[Pt(mnt)$_2$] (**3**) with 50% probability thermal ellipsoids (M stands for Ni or Pt).

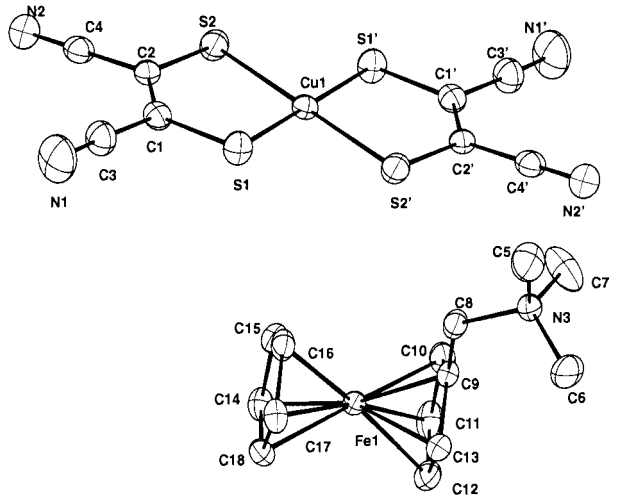

Figure 2. Atomic numbering scheme for ($FcCH_2NMe_3$)$_2$[Cu(mnt)$_2$] (**4**) with 50% probability thermal ellipsoids.

The canting of the anion plane and its zigzag arrangement along the c axis make the modes of overlapping between adjacent molecules within the [M(mnt)$_2$]$^-$ column markedly different (Figure 4a and b).

The shift between molecules A and B is mainly along the x axis of the molecule and the metal atom is roughly positioned over the ring C−S bond (Figure 4a). The shift between molecules B and A′ is mainly along the y molecular axis, and in this case one of the sulfur atoms is located nearly over the ring of the adjacent molecule (Figure 4b). Several M···S and S···S short contacts essential for the intermolecular interaction can be found between the AB and A′B pairs (Table 2). In the first instance, one type of short S(3)···S(4) contacts equal to 3.565(1) or 3.640(4) Å and one M···S(4) contact equal to 3.648 or 3.688 Å were observed for complexes **2** and **3**, respectively (see Figure 3). For the second overlapping mode, the shortest S(1)···S(4) distance is considerably longer, 3.795 or 3.770 Å, respectively, while the M···S(4) contact is shorter for the Ni compound (3.527 Å) and slightly shorter (3.626 Å) for the Pt complex.

(13) Sheldrick, G. M. *SHELXS86: Program for the Solution of Crystal Structures*; University of Göttingen: Federal Republic of Germany, 1986.
(14) Carruthers, J. R.; Watkin, D. J. *Acta Crystallogr., Sect. A* **1979**, *35*, 698−699. Prince, E. *Mathematical Techniques in Crystallography and Material Sciences*; Springer: New York, 1982.
(15) Watkin, D. J.; Prout, C. K.; Carruthers, R. J.; and Betteridge, P. W. *CRYSTALS*; Chemical Crystallography Laboratory: Oxford, U.K., 1996; Issue 10.
(16) Cromer, D. T.; Waber, J. T. *International Tables for X-ray Crystallography*; Kynoch Press: Birmingham, U.K., 1974; Vol. 4.

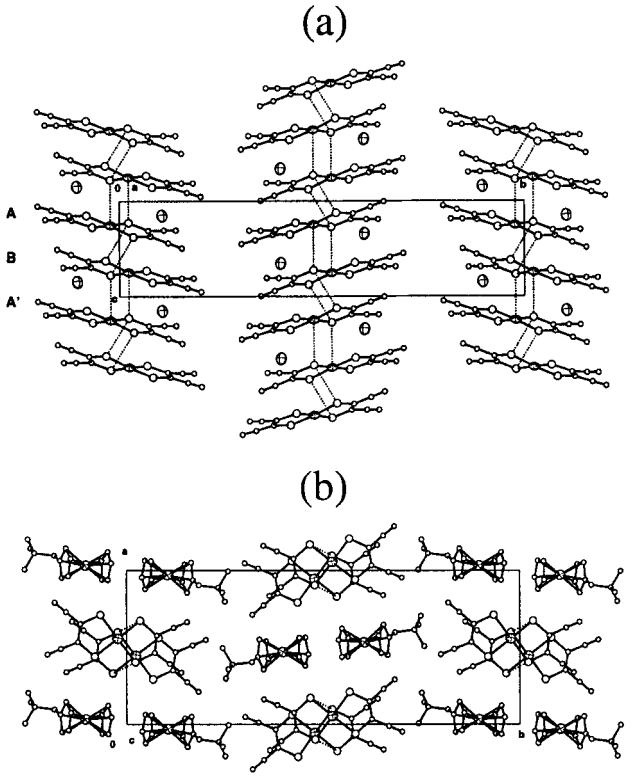

Figure 3. Projection of the structure of (**3**) along the *a* axis (a) and along the *c* axis (b) at 295 K. Dotted lines indicate short S···S contacts (<3.70 Å) and M···S contacts (3.527 and 3.626 Å for **2** and **3**, respectively).

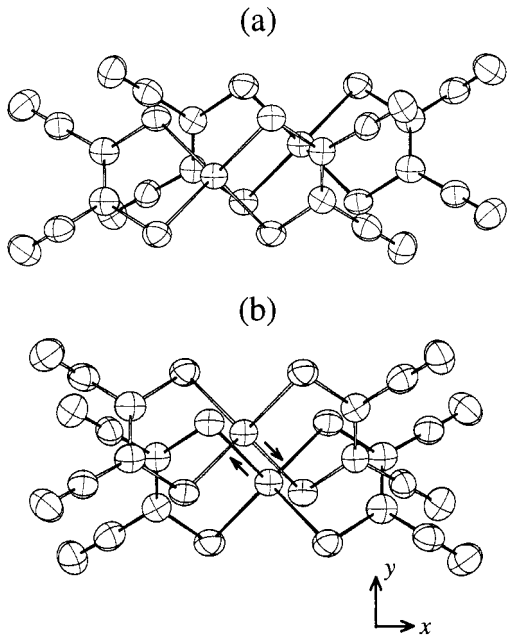

Figure 4. Modes of overlapping in **3**: (a) between A and B; (b) between B and A′ at 295 K (A, B, and A′ refer to the Figure 3).

Although $(FcCH_2NMe_3)_2[Cu(mnt)_2]$ (**4**) has a 2:1 stoichiometry, the packing of the anionic units are markedly different from compounds **2** or **3**. As a Cu atom is in a special position of the asymmetric unit, the dianions $[Cu(mnt)_2]^{2-}$ are completely isolated with no intermolecular interactions observed. The $[Cu(mnt)_2]^{2-}$ entities lie on the corners and in the center of the cell (Figure 5). The perpendicular to the mean planes of the anions forms angles of 53.4° and 41.8° with the *a* and *b* directions (Figure 5) and are almost perpendicular to the *c* direction (Figure 6). The cations lie between the $[Cu(mnt)_2]^{2-}$ planes.

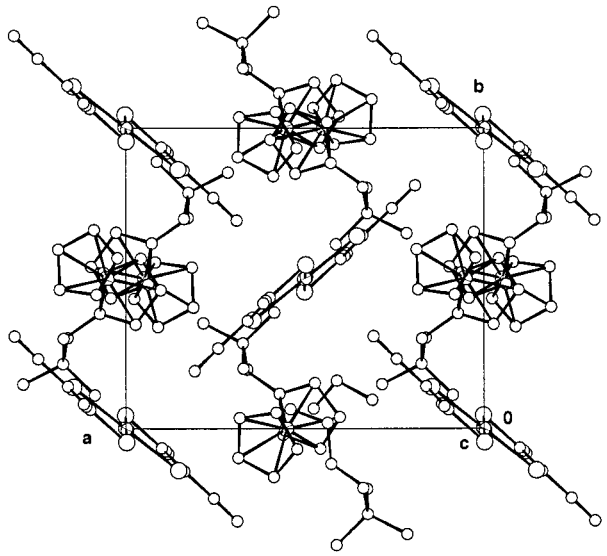

Figure 5. Projection of the structure of **4** along the *c* axis.

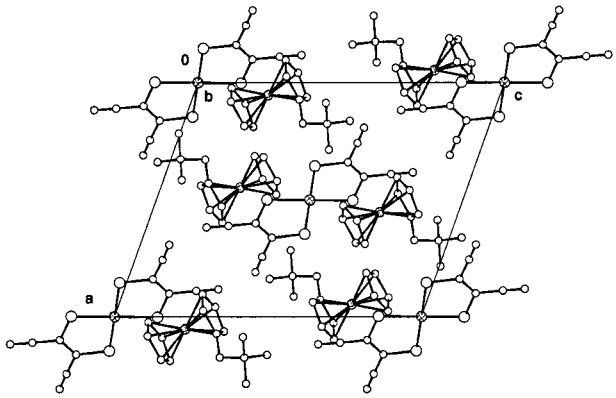

Figure 6. Projection of the structure of **4** along the *b* axis.

Unlike in **2** and **3**, the dianions in **4** do not stack in columns, but the planes of the dianions are at 96.5° with respect to each other. The closest inter-dianionic distances as well as the shortest dianion−cation contacts are far beyond that at which the van der Waals interaction would be observed. Thus, in the $(FcCH_2NMe_3)_2[Cu(mnt)_2]$ (**4**) compound, $[Cu(mnt)_2]^{2-}$ anion radicals are magnetically isolated from each other as well as from the $FcCH_2NMe_3^+$ cations.

Magnetic Properties. The temperature dependence of the molar magnetic susceptibility (χ_M) (represented in the form of $\chi_M T$ versus T) of $(FcCH_2NMe_3)[Ni(mnt)_2]$ (**2**) and $(FcCH_2NMe_3)[Pt(mnt)_2]$ (**3**) is shown in Figures 7 and 8, respectively. The room-temperature magnetic moments of Ni and Pt complexes (0.73 and 0.89 μ_B, respectively) are strongly reduced from the expected spin-only value of 1.73 μ_B.

For both compounds, the magnetic susceptibility decrease on cooling indicates an antiferromagnetic (AF) interaction between $[M(mnt)_2]^-$ units. At approximately 250 K the susceptibility of $(FcCH_2NMe_3)[Pt(mnt)_2]$ (**3**) drops abruptly (insert in Figure 8) indicating that the compound undergoes a phase transition. The transition temperature (T_p) at 247 ± 0.5 K was evaluated as the temperature at which the maximum of the $d\chi_M/dT$ derivative was observed. The transition is reversible and no sizable hysteresis (more than 1 K) was found.

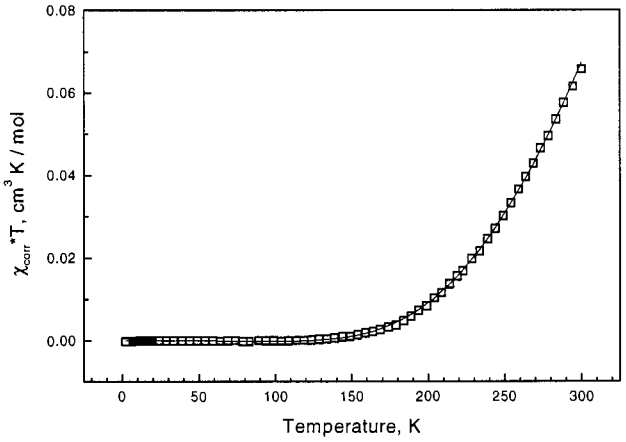

Figure 7. Experimental (□) and calculated (−) temperature dependence of χT for ($FcCH_2NMe_3$)[Ni(mnt)$_2$] (**2**) (see text for fit parameters).

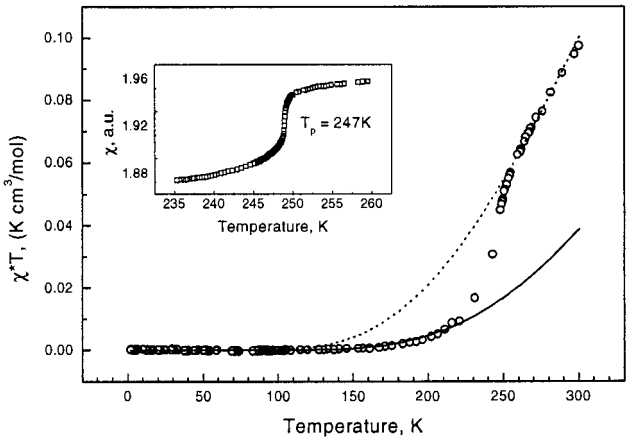

Figure 8. Experimental (○) and calculated (- - - for $J = -700$ cm^{-1}; — for $J = -900$ cm^{-1}) temperature dependence of χT for ($FcCH_2NMe_3$)[Pt(mnt)$_2$] (**3**). Inset: experimental (□) temperature dependence of χ in the vicinity of the phase transition temperature.

At low temperatures ($T < 100$ K), the data can be fitted to $\chi T = \chi_D T + C$ (subtracted in the Figures 7 and 8). The term $\chi_D = -1.26 \cdot 10^{-4}$ or $-1.71 \cdot 10^{-4}$ (cm^3/mol) represents a core diamagnetism and the constant $C = 0.0012$ or 0.001(K cm^3/mol), is a contribution of paramagnetic impurities obeying the Curie law, for Ni- and Pt-based compounds, respectively.

It should be noted that χ_D values are much lower than those values estimated from Pascal's constants (-3.15×10^{-4} for both compounds). This may be due to a large contribution of temperature independent paramagnetism of Ni(II) or Pt(II) ions. From the Curie constant values, we have estimated an $S = {}^1/_2$ impurity concentration in our samples of about $1 \pm 0.3\%$ for both compounds, assuming that the impurities have the same molecular weight and g factor as the actual compound. A preliminary ESR study of a single crystal of compound **2** shows that the paramagnetic contribution to the magnetic susceptibilty most probably originates from a small amount of noncoupled Ni(mnt)$_2$ anion radicals, frequently observed for polymetallic compounds.[17]

In contrast to compounds **2** and **3**, the magnetic susceptibility of ($FcCH_2NMe_3$)$_2$[Cu(mnt)$_2$] (**4**) strictly obeys the Curie law. Such behavior is consistent with the structure of this compound in which [Cu(mnt)$_2$]$^{2-}$ anions are completely magnetically isolated.

(17) Kahn, O. *Molecular Magnetism*; VCH: New York, 1993; Chapter 6.

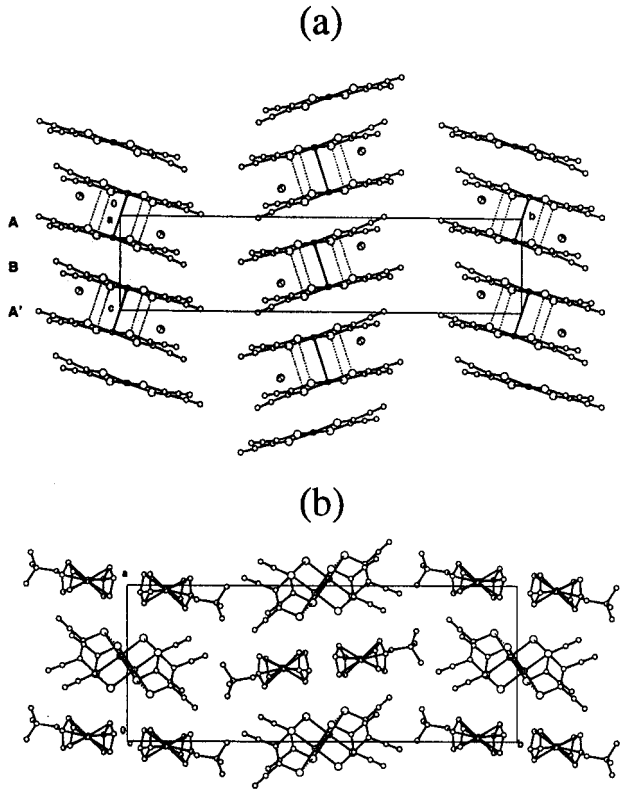

Figure 9. Projection of the structure of **3** along the *a* axis (a) and along the *c* axis (b) at 160 K. Dotted lines indicate short S· · ·S contacts (<3.70 Å).

Crystal Structure of ($FcCH_2NMe_3$)[Pt(mnt)$_2$] at 160 K. As mentioned above, ($FcCH_2NMe_3$)[Pt(mnt)$_2$] (**3**) undergoes a phase transition at 247 K. In order to clarify the structural changes of this compound we have performed X-ray diffraction data collection at 160 K, well below the transition temperature. The crystallographic data and data collection and processing parameters are presented in Table 1. The asymmetric unit and the labeling scheme are the same as shown in Figure 1. Selected M···M, M···S, and S···S intermolecular distances for this compound at 160 K are shown in Table 2.

Comparing the crystallographic parameters at 160 K and room temperature, one can see that the system preserves its lattice space group and the changes in the lattice parameters are small. The main motive of the crystal packing (columns of anions along the *c* direction separated by columns of cations) also remains the same at low temperature (Figure 9a and b). However, the arrangement of planar [Pt(mnt)$_2$] anions in the column are very different. At 160 K, the stack canting angle increases (the angle between the perpendicular to the plane of the [Pt(mnt)$_2$]$^-$ entity in the column and the *c* direction) increases from 13.8° to 18.0°.

The central Pt atoms are still positioned in an alternating zigzag fashion (A−B−A′), but the distance between central metal atoms of the anions A and B (4.418 Å) is now much larger than between anions B and A′ (3.451 Å). This indicates that anions A′ and B have moved toward each other along the *c* direction. Since the molecules A and A′ are equivalent, the distance between molecules A and B increases. In fact, at 160 K the [Pt(mnt)$_2$]$^-$ columns become dimerized.

The modes of overlapping between adjacent anions within the dimer (molecules A′ and B) and between the dimers (molecules A and B) are completely different (Figure 10a and b). The interdimer overlapping is practically the same as the overlapping observed at room temperature between molecules

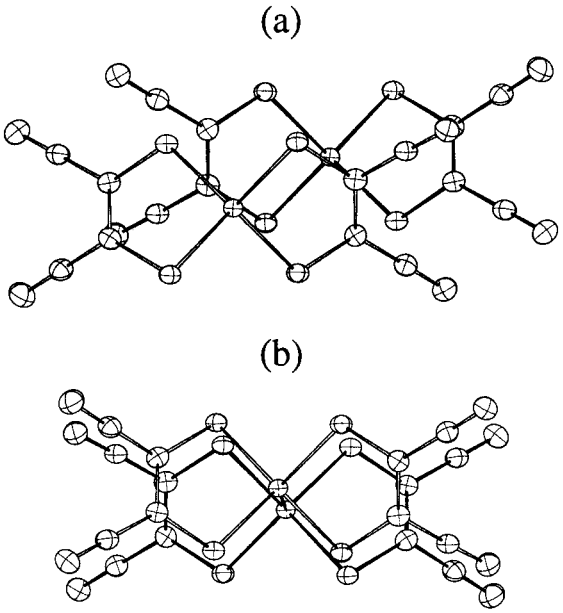

Figure 10. Modes of overlapping in **3**: (a) between A and B; (b) between B and A′ at 160 K (A, B, and A′ refer to the Figure 3).

A and B, the metal atom being still positioned over the C−S bond (Figure 10a). Within the dimer, the molecules A′ and B are arranged "face-to-face" in a nearly eclipsed configuration (Figure 10b). This means that as a result of the phase transition, the molecules A′ and B have slipped (near 0.2 Å) with respect to each other along one of Pt−S bonds (these displacements are shown by arrows in Figure 4b) and become almost eclipsed. In addition to the Pt−Pt "bond" (3.451(1) Å) formation there are two types of short S···S contacts, 3.408(1) and 3.534(1) Å, which have formed in the dimer (see Figure 9a).

To obtain additional information about the thermodynamic properties of the observed phase transformation, DSC measurements on $(FcCH_2NMe_3)[Pt(mnt)_2]$ (**3**) were performed. The heat-flux DSC trace at the warming rate of 10 K/min is shown in Figure 11.

At 247 K an endothermic process is observed. The endothermic effect of this transition (the enthalpy change, ΔH) is about 0.858 J/mol. Therefore, we can conclude that the observed phase transition is first order, and the low-temperature phase is about 8.9 meV ($\sim$72 cm^{-1}) lower in potential energy than the high-temperature one.

General Discussion

As described above, at room temperature the $[M(mnt)_2]^-$ (M = Ni, Pt) columns consists of the slipped anion pairs interacting through the M···S contacts. According to Alvarez et al.,[18] the ligand−ligand interaction is repulsive in character and a slipped arrangement of the pair is an efficient way to relieve this repulsion. On the other hand, an attractive or bonding interaction within a pair occurs due to overlapping of a d_{xz} orbital of metal (which is substantially admixed to the LUMO) with a p_z orbital of sulfur.[19] Since the d_{xz} orbital is directed into the ring in the *xz* plane of the molecule, one can assume that the sulfur-over-ring overlapping mode between molecules A′ and B provides a more efficient intermolecular coupling than the metal-over-C−S bond overlapping in the AB case.

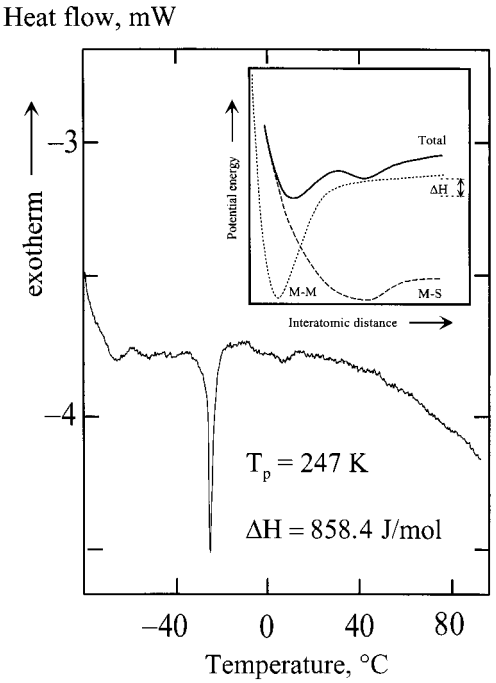

Figure 11. Differential scanning calorimetry of $(FcCH_2NMe_3)[Pt(mnt)_2]$ (**3**) showing the phase transition at 247 K.

The decrease of $\chi_M T$ in the 300−120 K temperature range clearly indicates that this interaction is antiferromagnetic in origin. In $(FcCH_2NMe_3)[Ni(mnt)_2]$ (**2**), it is so strong (M···S contact is 3.527 Å) that the compound is already diamagnetic below 120 K and the triplet state is totally depopulated. On the other hand, the interaction between molecules A and B is apparently much smaller (M···S contact is only 3.648 Å) and the A′B pairs could be considered as magnetically isolated. Presuming that we are dealing with an array of AF-coupled weakly interacting pairs, one can describe the electronic properties of such system with the Hubbard model.[20] The spin dependent part of the Hubbard Hamiltonian can be rewritten as the Heisenberg Hamiltonian. From the susceptibility data one can easily deduce the AF exchange parameter *J*. The expression for $\chi_M T$ is as follows,[17]

$$\chi_M T = 2N\beta^2 g^2/k[3 + \exp(-J/kT)] \quad (1)$$

where *g* is the Zeeman *g* factor of the $[Ni(mnt)_2]^-$ unit and was taken to be equal to 2.1. The best fit of the experimental data (solid line in the Figure 7) was obtained for $J = -840$ cm^{-1}.

As is well-known, the Hubbard model allows one to express the AF exchange energy *J* (<0, singlet−triplet energy gap) in terms of the on-site Coulomb repulsion (*U*) and the electron-transfer energy (*t*). The long-range Coulomb interaction is neglected in this model.

$$J = U/2 - (U^2/4 + 4t^2)^{1/2} \quad (2)$$

On the other hand, the energy of the charge-transfer transition ($h\omega_{CT}$) is equal to

$$h\omega_{CT} = U/2 + (U^2/4 + 4t^2)^{1/2} \quad (3)$$

Combining these two equations one can obtain expressions for

(18) Alvarez, S.; Vicente, R.; Hoffman, R. *J. Am. Chem. Soc.* **1985**, *107*, 6253−6277.
(19) Herman, Z. S.; Kirchner, R. F.; Loew, G. H.; Mueller-Westerhoff, U. T.; Nazzai A.; Zerner, M. C. *Inorg. Chem.* **1982**, *21*, 46−56.
(20) Bozio, R.; Pecile, C. *Spectroscopy of Advanced Materials*; Clark, R. J. H., Hester, R. E., Eds.; John Wiley & Sons Ltd.: Chichester, U.K., 1991; Chapter 1 and references therein.

t and *U* in terms of *J* and $h\omega_{CT}$.

$$4t^2 = |J| \cdot h\omega_{CT} \text{ and } U = h\omega_{CT} - |J| \quad (4)$$

Taking the $h\omega_{CT}$ value of 7200 cm^{-1} from the optical studies of $(NEt_4)[Ni(mnt)_2]$[21] and the *J* value from our magnetic experiments, one can evaluate that $t = 1230$ cm^{-1} and $U = 5970$ cm^{-1}. Although the *t* value does not obey the $U \gg 4t$ criterion, minimally, it gives us a quantitative insight into the electronic structure of this compound.

The interpretation of the magnetic properties of $(FcCH_2NMe_3)[Pt(mnt)_2]$ (**3**) (Figure 8) is not so straightforward. At room temperature, this complex has a higher value of $\chi_M T$ than the Ni derivative. According to our model it suggests a smaller AF exchange parameter *J*, which is consistent with a slightly larger value of M···S contacts between the $Pt(mnt)_2$ anions within the A′B pair (3.527(1) Å for Ni and 3.626(4) Å for the Pt complex).

Below 220 K, the $\chi_M T$ values are even smaller than in the Ni-compound implying an increase of *J* absolute value below the transition. This fact is again consistent with observed structural changes in the low-temperature phase of $(FcCH_2NMe_3)[Pt(mnt)_2]$ (**3**) in which Pt−Pt bonded $[Pt(mnt)_2]_2^{2-}$ dimers are observed. Unfortunately, the range of the $\chi_M T$ changes below and above the transition temperature is too small to be fit to eq 2 with suitable confidence, and the dashed ($J = -700$ cm^{-1}) and solid line ($J = -900$ cm^{-1}) curves are shown for qualitative comparison (Figure 8).

As it was pointed by Alvarez et al.,[18] the choice between two alternative dimeric structures (slipped and eclipsed) relied on a delicate balance between M···S or M···M bonding and inter-ring repulsion. In fact for the $(FcCH_2NMe_3)[Pt(mnt)_2]$ (**3**) compound the realization of both of these dimeric structures were observed. On the basis of this hypothesis, we can propose the following scenario of the $(FcCH_2NMe_3)[Pt(mnt)_2]$ (**3**) behavior on cooling. Above T_p, the inter-ring repulsion exceeds the Pt···Pt attraction and a slipped configuration is realized just to relieve this repulsion. On cooling the lattice contracts, the Pt···Pt distances decrease and the attraction begins to dominate. This interaction "drags" the $[Pt(mnt)_2]^-$ anions along the Pt−S bond (as it is shown in Figure 4a). Finally below the transition temperature, the eclipsed configuration of the $[Pt(mnt)_2]_2^{2-}$ dimers is achieved and a new balance between Pt···Pt attraction and inter-ring repulsion is established. The Pt−Pt distance is much shorter in this case and the AF exchange more efficient. To illustrate the mechanism of the phase transformation described above, schematic potential energy curves representing the contributions of the two attractive Pt···Pt and Pt···S interactions as well as a composite total energy curve can be drawn (insert in Figure 11). One can see that the system has two shallow minima, and the difference between their energies corresponds to the observed ΔH value in our DSC experiment.

In fact, this value correlates well with the changes in the AF exchange energy *J*. Since the $h\omega_{CT}$ is mainly determined by *U*, which in turn is a characteristic of the molecule itself, we can assume that it has nearly the same value in the low and high-temperature phases. Therefore, using eq 4 and the evaluated values for *J* (−900 and −700 cm^{-1} for low- and high-temperature phases, respectively) we can estimate a difference in the electron-transfer energy, Δt of about 150 cm^{-1}. Taking into account that some energy is probably consumed for minor changes of the anion geometry, then the correlation with ΔH (72 cm^{-1}) is quite reasonable. Since *t* is a measure of the intermolecular bonding interaction, we can conclude that in the eclipsed arrangement $Pt(mnt)_2$ anions in the dimer are more strongly interacting than the pairs in the slipped configuration. On the other hand, the difference in bonding is so slim that any of these arrangements could be realized simply by changing of the cation, synthesis conditions, solvents, etc. It should be noted that the minimum of the free energy in the low temperature state should be in fact quite shallow (about kT_p) since the phase transition is reversible.

In the case of the Ni compound, the Ni···Ni bonding distance is much smaller than for Pt and thus, the $[Ni(mnt)_2]^-$ pairs apparently remain in a slipped configuration throughout the entire investigated temperature range.

Conclusions

As was mentioned in the Introduction, the main goal when we initiated this work was to design metal dithiolene-based molecular based magnetic materials with larger dimensionality than those already reported using a bulky ferrocenium-based cation. Our goal was not achieved as the synthesized compounds exhibit a singlet ground state (for Ni and Pt dithiolenes) implying one-dimensional character of intermolecular coupling within the $[M(mnt)_2]^-$ chains and very small (if any) interchain interaction. In the Cu dithiolene-based compound $(FcCH_2NMe_3)_2[Cu(mnt)_2]$ (**4**), the anion radicals are completely magnetically isolated. On the other hand, it was found that the $(FcCH_2NMe_3)[Pt(mnt)_2]$ compound exists in two different phases which reversibly transforms into each other at $T_p = 247$ K. In the high-temperature phase the anionic chain consists of Pt···S-coupled, slipped $[Pt(mnt)_2]^-$ pairs and the low-temperature one is characterized by the presence of Pt···Pt coupled $[Pt(mnt)_2]_2^{2-}$ dimers in an eclipsed configuration. Detailed monitoring of the structure changes occurred as a result of the phase transformation together with the analysis of the magnetic properties allowed us to propose a mechanism for this phase transition.

Acknowledgment. We would like to thank the Ministere Affaires Etrangères of the French Government for a Chateaubriand Fellowship for A.E.P. and also the Centre National de la Recherche Scientifique for a "Chercheur Associé" fellowship for K.I.P. Technical assistance of M. Benoist (Setaram Company) in DSC experiments is aknowledged.

Supporting Information Available: X-ray crystallographic files, in CIF format, for the structure determinations of **2**, **3**, and **4** are available on the Internet only. Access information is given on any current masthead page.

IC980876V

(21) Kutsumizu, S.; Kajima, N.; Watanabe, N.; Ban, T. *J. Chem. Soc., Dalton Trans.* **1990**, 2287−2292.